JOURNAL OF SOLID STATE CHEMISTRY 88, 351–367 (1990)

The Chemistry of the Thermal Decomposition of Pseudobrookite Ferrous Titanium Oxides

RAYMOND G. TELLER AND MARK R. ANTONIO

BP Research, Warrensville Laboratory, 4440 Warrensville Center Road, Cleveland, Ohio 44128-2837

ALPHONSO E. GRAU AND MICHEL GUEGUIN

QIT-Fer et Titane Inc., P. O. Box 560, Sorel, Quebec Canada J3P 5P6

AND EDWARD KOSTINER

Department of Chemistry, University of Connecticut, Storrs, Connecticut 06269

Received February 12, 1990; in revised form May 11, 1990

The thermal decomposition of two metastable ferrous titanium oxide compounds of commercial interest have been studied by *in situ* X-ray and neutron diffraction at elevated temperatures as well as by ^{57}Fe Mossbauer effect spectroscopy. Thermal decomposition was monitored by collecting neutron diffraction data (taken at the Argonne National Laboratory Intense Pulsed Neutron Source (IPNS) powder diffractometers) at 30-min intervals at 900 and 1000°C. Previous work has shown that each of these materials (pseudobrookite structure, AB_2O_5), $(Mn_{0.05}Fe_{0.33}Ti_{0.52})(Ti_{2.0})O_5$ and $(Mg_{0.21}Fe_{0.33}Ti_{0.46})$-$(Ti_{1.9}Mg_{0.1})O_5$, has a significant amount of Ti in the +3 oxidation state and is completely ordered (no Fe located in the "*B*" site). The results of these "in situ" diffraction studies show that, prior to the thermal decomposition of the slags, there is a redistribution of cations within the pseudobrookite structure. Specifically, at temperatures in the range 600–700°C, iron cations move from the "*A*" sites to the "*B*" sites and Ti cations move from the "*B*" to the "*A*" sites. It is after this order–disorder transition that decomposition commences. At temperatures above 900°C, the neutron diffraction data show at least two modes of decomposition describing the high temperature chemistry of these disordered materials. The first mode produces iron metal and rutile (TiO_2) and is modeled by the equation

$$2Fe_{0.5}Ti_{2.5}O_5 \rightarrow Fe + 5TiO_2.$$

The second mode of decomposition produces an iron-doped titanium oxide of the rutile structure and is modeled by the equation

$$4M_{0.3}Ti_{2.7}O_5 \rightarrow 2M_{0.5}Ti_{2.5}O_5 + 5Fe_{0.04}Ti_{1.16}O_2 \ (M = Fe^{2+}, Mn^{2+}, Mg^{2+}).$$

© 1990 Academic Press, Inc.

Introduction

During the course of structural investigations of ferrous titanium oxides with the pseudobrookite (AB_2O_5) structure (*1*), it was noted that the temperature of preparation and the conditions of reduction largely determined the distribution of metal atoms within the AB_2O_5 structure. Neutron diffraction and ^{57}Fe Mossbauer effect spectros-

0022-4596/90 $3.00

Copyright © 1990 by Academic Press, Inc.
All rights of reproduction in any form reserved.

copy studies of titanium-rich compounds ($Fe_{1-x}Ti_{2+x}O_5$, $x > 0$) prepared at low temperatures (1200°C) demonstrated that ferrous ions are distributed between both *A* and *B* sites (*1, 2*), whereas studies of compounds prepared at higher temperatures (>1700°C) under carbon monoxide atmospheres found ferrous ions only at the *A* site (*1*). It is well known that these materials are metastable. For example, it has been shown that $FeTi_2O_5$ is thermodynamically unstable with respect to $FeTiO_3$ and TiO_2 (*3*), and that titanium-rich compounds, which necessarily possess both Fe^{2+} and Ti^{3+} cations, are unstable with respect to the metals in their 0 and +4 oxidation states, respectively (*4*).

Based on these observations, an *in situ* high temperature diffraction study of the decomposition of pseudobrookite materials that were prepared at elevated temperatures (above 1700°C) was undertaken. Two samples were studied by powder X-ray and neutron diffraction: slag I and slag II. These are commercial samples synthesized by the high temperature reduction of ilmenite ore. These titanium-rich ($M^{2+}_{1-x}Ti_{2+x}O_5$) materials differ in the identity of the M^{2+} cation; in slag I, M = Fe and Mn, $x = 0.52$, and in slag II, M = Fe and Mg, $x = 0.36$.

This work consists of *in situ* powder X-ray diffraction experiments at several temperatures to determine the temperatures at which changes in slags I and II occur, and *in situ* powder neutron diffraction experiments at 900°C for slag I and at 1000°C for slag II to determine the detailed chemistry of the decomposition process for each of these samples at these temperatures. Diffraction data were analyzed by the Rietveld technique (*5*), a least-squares fitting process in which models for all contributions to the diffraction pattern are fit to observed diffraction data. Rietveld analysis is well suited to extract structural information from powder diffraction data. (*6*). Also, zero-field, ^{57}Fe (natural abundance) Mossbauer effect data were obtained for slags I and II after the high temperature neutron diffraction experiments.

Neutron diffraction offers two distinct advantages over X-ray diffraction for these particular studies. The first advantage is due to the difference between X-ray and neutron scattering physics. Since X-rays are scattered by electron density, the similarity of the atomic numbers of iron and titanium makes distinguishing between these elements difficult in an X-ray scattering experiment. Neutrons, however, are scattered by nucleii, and it happens that Ti and Fe possess very different neutron scattering lengths (-0.33×10^{-12} and 0.95×10^{-12} cm, respectively). This large difference allows the distinction between these metals necessary for this work. The second advantage results from the disparity of X-ray and neutron absorption coefficients. With the exception of a few elements (cadmium, lithium, etc.), neutron absorption coefficients are orders of magnitude smaller than X-ray absorption coefficients in the wavelength range of interest (1.0–3.0 Å). Since furnaces mounted on diffractometers necessarily have shielding of some kind to maintain internal temperatures, the quality of X-ray diffraction data collected at elevated temperature is degraded due to absorption of X-rays by this shielding. But because corresponding thermal neutron absorption coefficients are much smaller, this degradation in data quality due to ancillary devices is much less severe for neutron data. In fact, if a well-designed furnace is employed, it is very difficult to distinguish between neutron diffraction data collected with and without a furnace.

Experimental

Samples slag I and slag II are commercial iron (magnesium) titanium oxide mixtures prepared by the reduction of ilmenite with carbon at temperatures above 1700°C. The process is roughly described by the follow-

ing equation:

$$2FeTiO_3 + C \rightarrow CO + FeTi_2O_5 + Fe. \quad (1)$$

At the synthesis temperatures, molten Fe is easily separated from the slag ($FeTi_2O_5$). For samples I and II, carbon in excess of that described by Eq. (1) was used in the reduction, producing a titanium-rich, $Fe_{1-x}Ti_{2+x}O_5$, material that is nearly 100% pure.

The difference between samples slag I and slag II is the presence of significant amounts of Mg in the starting material for II and small amounts of Mn in I. Elemental analyses (XRF) of I and II yield the following stoichiometries (based on 5 oxygen atoms): $Ti_{2.52}Fe_{0.33}Mn_{0.05}O_5$ and $Ti_{2.36}Fe_{0.33}Mg_{0.31}O_5$, respectively.

Neutron diffraction measurements. Time-of-flight (TOF) neutron diffraction data were collected at ambient pressure at Argonne National Laboratory with the IPNS (Intense Pulsed Neutron Source) on the special environment powder diffractometer. Data from the backscattering detectors ($2\Theta = 150°$) were used in the refinements as this is the highest resolution data available from each instrument (ca. 0.3%). In the TOF technique, the sample, detector, and source are fixed and neutrons of differing wavelengths are detected. The data are binned in 5-μsec intervals. Each sample was contained within a 1/2-in.-diameter seamless vanadium tube (due to the very small scattering length of vanadium, this renders the sample holder virtually invisible), capped at both ends with aluminum plugs. Details of the instrument and the data collection and data analysis software package have been previously published (*7*).

The neutron experiments were conducted in a locally designed and constructed furnace. The sample is held in a vanadium cylinder and resistance heating raises the temperature of the sample. The entire sample chamber was maintained at pressures below 10^{-4} Torr throughout the course of the experiment. Thermocouples placed at each end of the cylindrical holder monitored the sample temperature. At no time during data collection did these two temperature readings differ by more than 5°C, or each vary by more than 3°C from the setpoint.

The experimental strategy employed for collection of the neutron diffraction data was as follows: an initial data set was collected (for 2 hr) at room temperature. Following this the temperature of the sample was gradually increased to 500°C, then raised to the desired set point (900 or 1000°C) as rapidly as possible (usually in about 2–4 min). The time at which the desired temperature was reached was arbitrarily designated $t = 0$ min. Data were then collected for 15 or 30 min at intervals separated by 1 or more hours. At the conclusion of each run, the sample was allowed to cool to room temperature, equilibrated for a minimum of 4 hr, and then another high precision data set taken (2-hr data collection time). Because the diffraction data taken at elevated temperature was collected for short periods (in order to get a "snapshot" of the state of the mixture), the precision of the results derived from these data sets do not match those of the first and last data sets. The results of these runs are summarized in Tables I and II. The final set point temperatures were 900 and 1000°C for slags I and II, respectively.

To extract kinetic as well as structural information from the neutron diffraction data, each data set was subjected to Rietveld analysis. The least-squares software utilized for the analysis was developed at Argonne National Laboratory and is written for time-of-flight neutron data and multiphase samples (*7c*). Starting structural parameters for the least-squares process were taken from the open literature. For the ferrous pseudobrookite structure, a crystallographic model isostructural with that of ferric pseudobrookite was chosen (*8*) (*Cmcm*, two metal sites, metal atoms at 4*c* 100% Ti, 0% Fe = 0.0, 0.19, 0.25 and 8*f* 50% Ti, 50% Fe = 0.0,

0.135, 0.56.) In the following discussion, the 4*c* site is designated as "*A*" and the 8*f* as "*B*". In the least-squares refinement, only the scale factors and background parameters were initially allowed to vary. Upon convergence, more parameters were added until, for the final cycles of least-squaring, all reasonable parameters were allowed to vary. They include isotropic thermal and atomic positional parameters, unit cell constants, background, and peak shape parameters. In addition to these, occupational parameters of the metal sites were also allowed to vary: each cation was refined as though it were a Ti atom. This is equivalent to refining the scattering length because the algebraic sum of the individual scatterers can be readily calculated. Oxygen occupancies were also varied for one set of least squares, and since the values did not differ significantly from zero they were subsequently fixed at 100%. Scattering lengths used in subsequent calculations are −0.33 for Ti, 0.95 for Fe, 0.52 for Mg, −0.36 for Mn, and 0.575 ($\times 10^{-12}$ cm) for O. Particularly important parameters to be gained from each Rietveld analysis are the scale factors (normalized to constant incident neutron flux) for each phase in each data set. These scale factors are directly proportional to the mole fraction of each phase (*9*) and the variation of the mole fraction of each phase as a function of time yields kinetic information regarding the solid state chemistry of the system.

In addition to pseudobrookite phases, titanium oxide (of the rutile structure) and iron were detected in each sample. These phases were present as impurities and also as decomposition products. Cell, positional, and thermal parameters for these phases were also allowed to vary, and as the titanium oxide content of each sample increased, the occupancy of the Ti atom site as well as an interstitial tetrahedral site were also allowed to vary. All refinements converged rapidly. Final plots showing the raw diffraction data, calculated data, and difference plots for selected patterns are given in Figs. 1–4.

X-ray diffraction data. X-ray diffraction data were collected on a Rigaku DMAXB powder diffractometer equipped with a rotating copper anode X-ray tube. The flat (19 × 16 mm) specimen was mounted vertically and para-focusing geometry was used in the data collection. The white X-ray beam is postsample graphite monochromatized. One degree divergence slits and a 0.3-mm receiving slit were used during data collection. The furnace utilized is a Rigaku-furnished device. The sample holder is platinum, and compression of the sample into ridges in the holder keep the powder in place. No reaction was detected between the sample holder and the sample at the conclusion of each experiment. Resistive heating is provided to the sample holder, and the sample holder temperature is monitored by a thermocouple. Temperature control was ±1°C. During the course of the experiments, the sample holder and its environment were continuously bathed in a stream of high purity nitrogen gas. Data collection was carried out by raising the temperature of the sample to the desired temperature, holding for 5 min and then collecting data over a narrow angular range ($14 < 2\Theta < 56$) in 15 min. Data were collected at 100°C intervals between 600 and 1300°C.

Mossbauer effect measurements. Zero-field, natural abundance iron-57 Mossbauer effect data were collected on the finely powedered slags (I and II after exposure to 900 and 1000°C, respectively) which were supported between boron nitride plates (1-in-diameter × 0.025-in.-thick PDS BN-975, Standard Oil Engineered Materials). The sample masses (ca. 0.28 g) were calculated to provide ideally-thin absorbers, ca. $1.0/(\mu/\rho)$, where μ/ρ is the nonresonant electronic mass absorption coefficient (cm^2/g) at 14.41 keV (*10*). A Ranger Scientific MS-900 Mossbauer effect spectrometer was em-

ployed for transmission measurements. The source (ca. 10 mCi cobalt-57 diffused into rhodium foil; Amersham) and slags were maintained at room temperature. The MS-900 was operated in the constant-acceleration mode using a triangular (symmetric) waveform to drive the Ranger Scientific VT-1200 velocity transducer. Velocity calibration over the region 0 ± 9 mm/sec was maintained by use of a natural iron, α-Fe, absorber foil (0.025 mm thick); all isomer shifts are quoted relative to natural iron at room temperature. The zero velocity calibration (i.e., 0 mm/sec isomer shift) was taken as the midpoint of the inner four resonances of the iron foil. A linear velocity scale was used for the velocity per channel (mm/sec/ch) conversion over the entire range. A Reuter-Stokes proportional counter (fill gas: 97% Kr–3% CO_2), fitted to a Ranger Scientific preamplifier (PA-900), and 1024 channel multichannel analyzer/scaler was used for the γ-ray detection. The entire MS-900 system was controlled with an IBM AT personal computer. All Mossbauer effect data were recorded to suitable background levels of ca. 2,100,000 and 1,300,000 counts per channel for slags I and II, respectively (after folding). The primary experimental data were folded and fit with Lorentzian line shapes. Estimated standard deviations for isomer shifts, quadrupole splittings, and FWHM (full width at half maximum) line widths are 0.02 mm/sec.

Results and Discussion

The pseudobrookite structure is adopted by a wide variety of metal oxides, particularly iron titanium oxides. The details of the structure have been reported elsewhere (*8*) and, for our purposes, only a summary of the key structural features require repeating here. A polyhedral representation of the structure is presented in Fig. 5. There are two distinct cation sites in the pseudobrookite AB_2O_5 structure situated such that *A* site metal oxygen octahedra edge and corner share only with *B* octahedra, whereas *B* sites edge and corner share with both *A* and *B* octahedra. Since all the *A* site second nearest neighbors are *B* sites, any cation exchange between *A* sites must be preceded by prior exchange with *B* sites.

The results of the X-ray diffraction experiments are illustrated in Figs. 6 (slag I) and 7 (slag II). Figures 6A and 7A illustrate the diffraction data of the high temperature quenched phases taken at room temperature. All large Bragg peaks are due to the dominant phase (pseudobrookite structure), with the largest impurity peak (rutile, TiO_{2-x}) indicated. This pattern remains unchanged (with the exception of shifting due to lattice parameter expansion) as the temperature is raised. Between 500 and 600°C, however, a dramatic change in the diffraction pattern occurs. This is illustrated in Fig. 6B. All of the peaks except two pseudobrookite peaks ([110] and [200]) are significantly broadened, despite the fact that the temperature is well below the melting point of this phase. This pattern is largely reproduced at 700 and 800°C (Figs. 6C and 6D) except that one can observe the growth of a decomposition product (rutile) at 800°C. At 900°C (Fig. 6E), the pattern has sharpened again, and the decomposition process has greatly accelerated as evidenced by the dominance of the Bragg peaks due to rutile.

This general pattern is repeated for slag II (Figs. 7A–7F). At 600, 700, and 800°C (Figs. 7B, 7C, and 7D, respectively) most of the Bragg peaks due to the pseudobrookite phase are broadened, and at 800°C one can observe the growth of the largest rutile Bragg peak. At 900 and 1000°C (Figs. 7E and 7F, respectively) the pseudobrookite peaks are once again sharpened and decomposition to rutile is greatly accelerated.

One possible explanation for the observed broadening of Bragg peaks at these low temperatures is rapid exchange of cations within

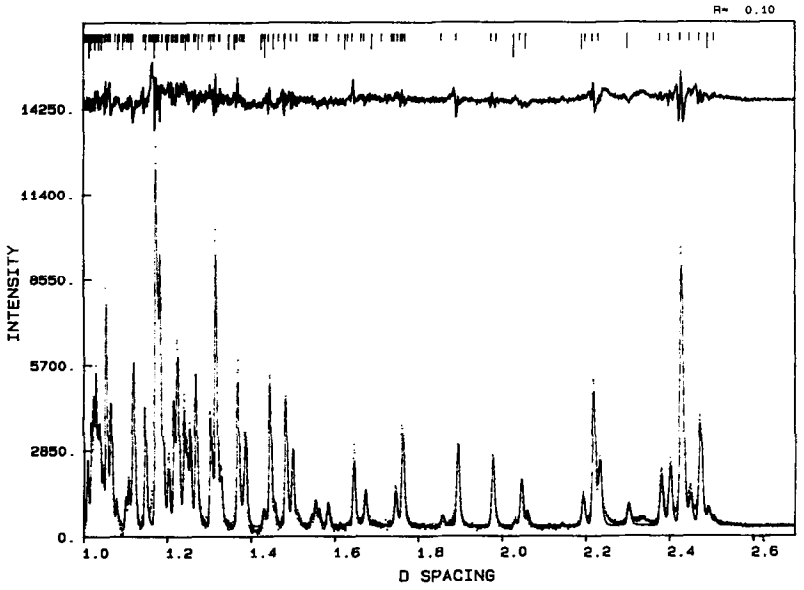

FIG. 1. A portion of the neutron diffraction data for slag I. Data is represented by points, and the calculated plot by a line. A difference plot is presented at the top of the figure. Tick marks indicate the positions of Bragg peaks. Three phases are present: pseudobrookite (short tick marks), rutile (TiO_2, longer tick marks), and iron metal (longest tick marks).

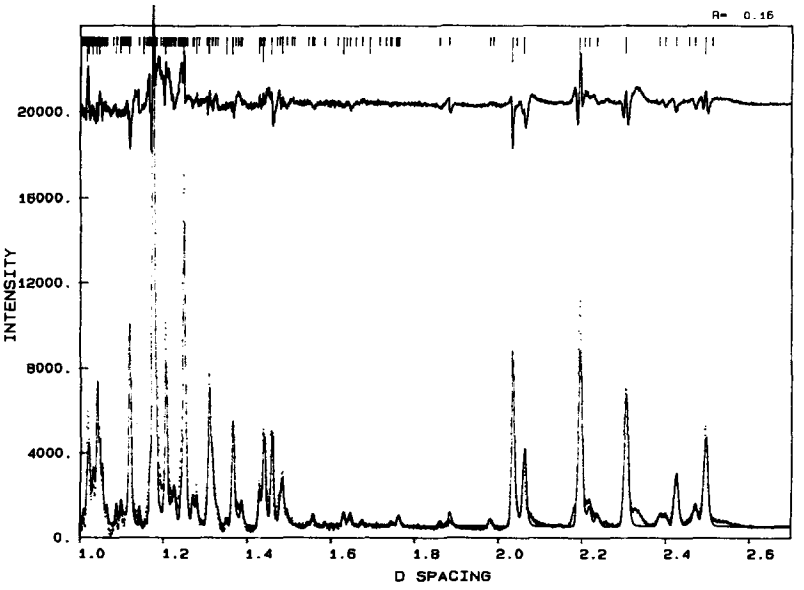

FIG. 2. Neutron diffraction data for slag I after 500 min at 900°C. Data is represented by points, and the calculated plot by a line. A difference plot is presented at the top of the figure. Tick marks indicate the positions of Bragg peaks as in the legend to Fig. 1.

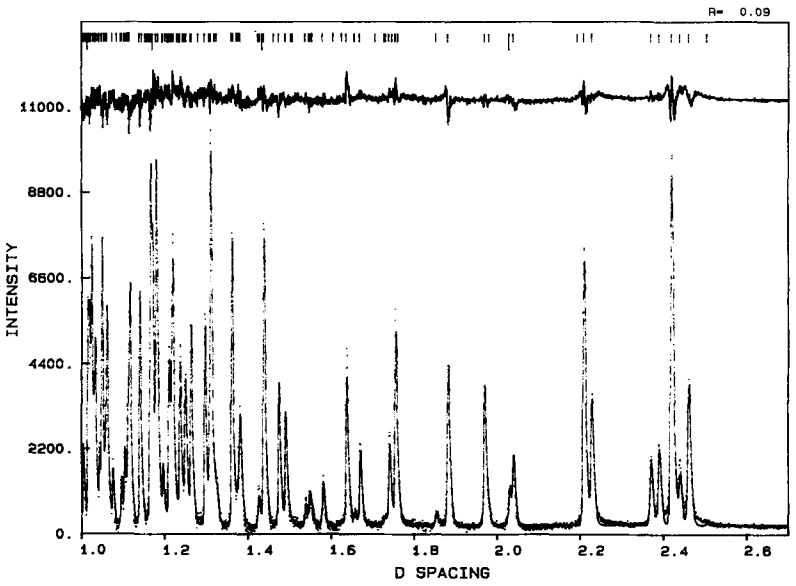

FIG. 3. Neutron data for slag II. Data is represented by points, and the calculated plot by a line. A difference plot is presented at the top of the figure. Tick marks indicate the positions of Bragg peaks. Two phases are present: pseudobrookite (short tick marks) and iron metal (long tick marks).

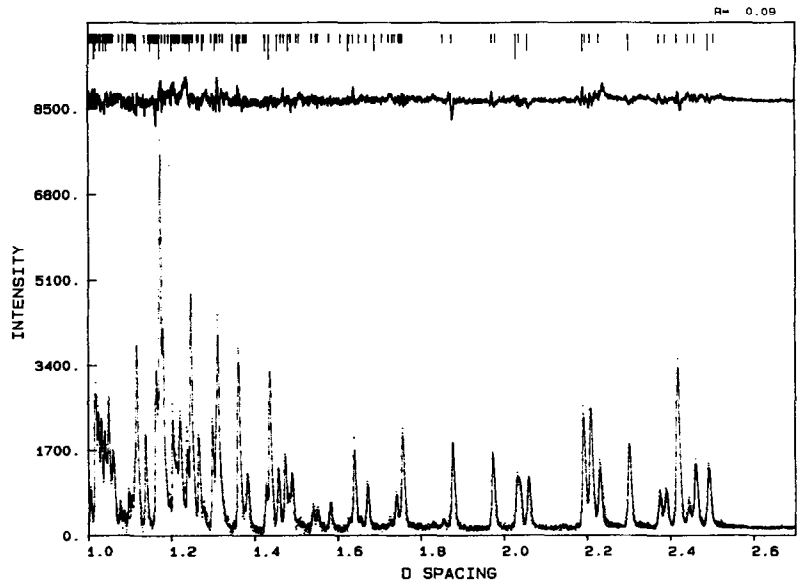

FIG. 4. Neutron data for slag II after 800 min at 1000°C. Data is represented by points, and the calculated plot by a line. A difference plot is presented at the top of the figure. Tick marks indicate the positions of Bragg peaks. Three phases are present: pseudobrookite (short tick marks), rutile ("TiO_2," longer tick marks), and iron metal (longest tick marks).

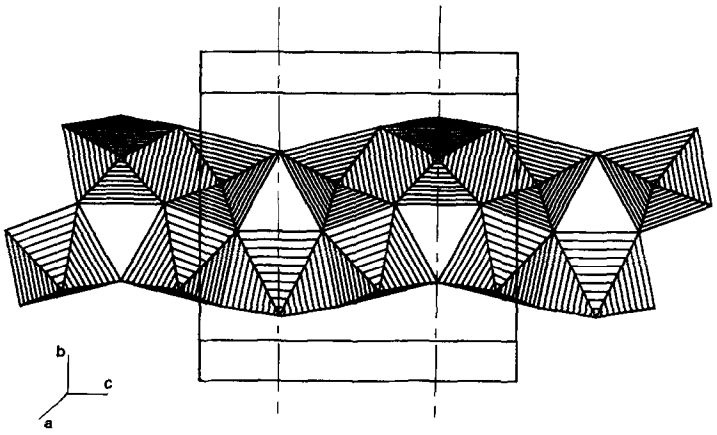

FIG. 5. Representation of the octahedral coordination polyhedra of the pseudobrookite (AB_2O_5) structure as viewed down a. A single chain of edge and corner-shared octahedra are shown. All cations are located on a mirror plane in the bc plane (a = 1/4). A sites lie on a line defined by the intersection of this mirror plane with mirror planes at b = 1/4 and 3/4. A sites share octahedron edges with B sites in sets of three. B sites are on the outside of each set of three edge-shared octahedra. The structure is generated by translating these chains by 1/2 unit cell in the a and b directions. Outlines of the unit cell are shown.

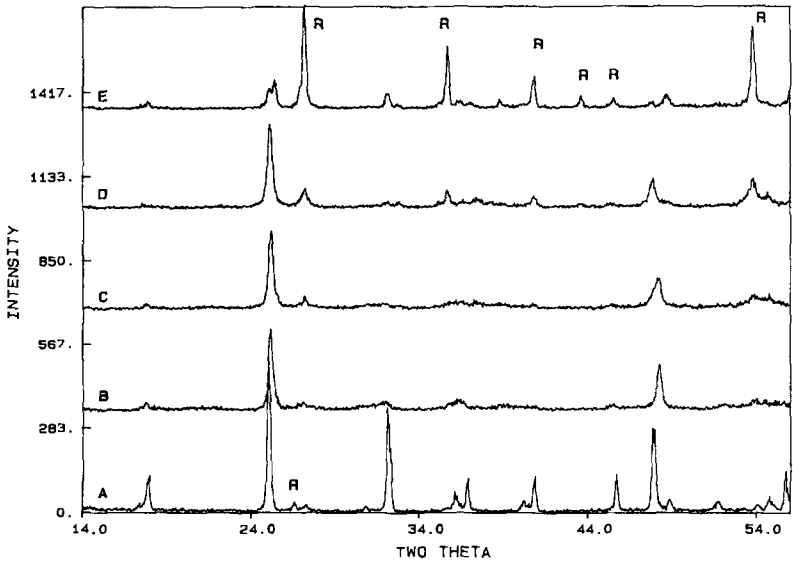

FIG. 6. (A) Room temperature X-ray diffraction data for slag I. The largest Bragg peak of the major impurity phase, TiO_2, is indicated by the letter "R". The remaining peaks are due to the pseudobrookite phase. (B) Slag I at 600°C, note the absence of numerous pseudobrookite Bragg peaks. (C) Slat I at 700°C; (D) Slag I at 800°C, and (E) Slag I at 900°C. Note that the most intense peaks in the pattern are due to a TiO_2 species (labeled with "R"), and pseudobrookite phase Bragg peaks are again sharp.

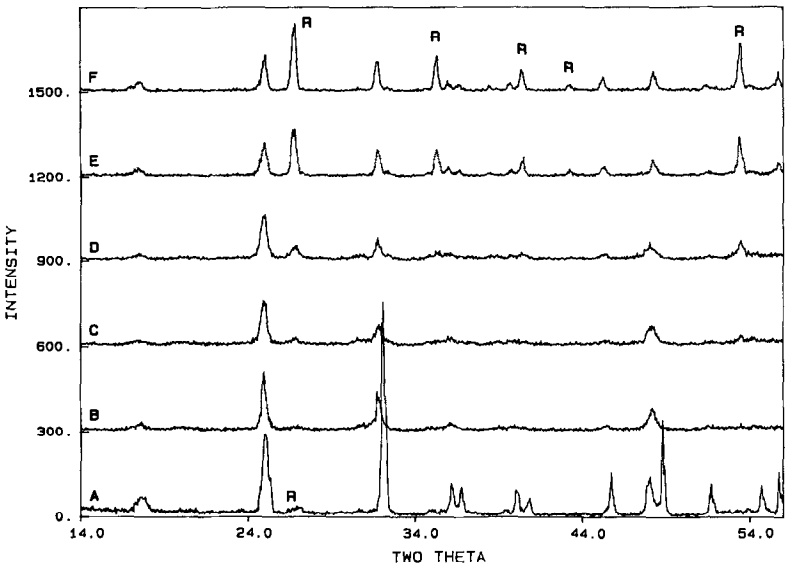

FIG. 7. X-ray diffraction data for slag II. As for Fig. 6, the letter "R" is used to mark TiO_2 Bragg peaks, while the remaining Bragg peaks are due to the pseudobrookite phase. (A) At room temperature, the major phase is pseudobrookite. At elevated temperatures (B–D) the pseudobrookite Bragg peaks diminish in intensity. At 900°C (E) decomposition of the pseudobrookite commences and all Bragg peaks are again sharpened with respect to lower temperatures.

the metastable pseudobrookite structure at temperatures above 500°C. Such a situation, in which the oxide lattice remains largely intact, and the long range ordering of the cations is lost due to rapid exchange between two exclusive cation ordering schemes, would give rise to the dramatic broadening observed. As the temperature is increased, the equilibrium mixture of these two phases changes until, at some temperature between 800 and 900°C, one of the two distributions dominates and the pattern begins to sharpen once again. Lastly, it is this final cation distribution that decomposes to rutile. The cation distribution of the original material (ferrous and titanium ions located on the *A* site, titanium only on the *B* site) is labeled the high temperature (HT) distribution because it is quenched from 1700°C. The second cation distribution which is stabilized at 900°C (vide infra) is labeled the low temperature (LT) distribution. This process is summarized in Eq. (2):

$$(AB_2O_5)_{HT} \overset{K}{\rightarrow}_{eq} (AB_2O_5)_{LT} \overset{k}{\rightarrow} \text{products.} \tag{2}$$

The hypothesis that this phase change occurs ($(AB_2O_5)_{HT} \rightarrow (AB_2O_5)_{LT}$) is supported by the neutron diffraction data. Some fits between the observed neutron diffraction data and calculated plots from Rietveld refinements are given in Figs. 1–4. Results of the refinements are summarized in Tables I–III. Table III shows that there are dramatic changes in scattering lengths of the two pseudobrookite cation sites as the temperature of these materials is raised. At room temperature the neutron scattering lengths of the *A* and *B* site for slag I are $0.09(1) \times 10^{-12}$ and $-0.33(1) \times 10^{-12}$ cm, respectively, whereas at 900°C the corresponding scattering lengths are $-0.06(2) \times 10^{-12}$ and $-0.28(2) \times 10^{-12}$ cm. Similar changes are also observed in the scattering lengths of the *A* and *B* sites for slag II. Exam-

TABLE I

RESULTS OF RIETVELD REFINEMENTS OF SLAG I AT DIFFERENT TEMPERATURES

Conditions	Pseudobrookite (*Cmcm*)		Titanium oxide ($P4_2/mnm$)		Iron
	Normalized scale factor	Unit cell	Normalized scale factor	Unit cell	Normalized scale factor
25°C	—	a = 3.7828 b = 9.7938 c = 10.0280	—	a = 4.6015 c = 2.9647	—
t = 0 900°C	0.083	a = 3.795 b = 9.924 c = 10.135	0.673	a = 4.642 c = 2.993	0.027
t = 60 min 900°C	0.052	a = 3.793 b = 9.924 c = 10.136	1.223	a = 4.642 c = 2.993	0.079
t = 120 min 900°C	0.042	a = 3.792 b = 9.920 c = 10.136	1.349	a = 4.642 c = 2.993	0.087
t = 180 min 900°C	0.039	a = 3.792 b = 9.920 c = 10.134	1.388	a = 4.642 c = 2.993	0.094
t = 375 min 900°C	0.031	a = 3.787 b = 9.913 c = 10.139	1.456	a = 4.642 c = 2.994	0.104
t = 510 min 900°C	0.030	a = 3.786 b = 9.912 c = 10.137	1.400	a = 4.642 c = 2.993	0.101
Exp. end 25°C	—	a = 3.7640 b = 9.8178 c = 10.0421	—	a = 4.6067 c = 2.9653	—

Note. Estimated standard deviations in lattice parameters are 0.002–0.003 for data taken at 900°C and 0.0002–0.0004 for data taken at 25°C.

ination of Table III also reinforces the strength of neutron diffraction as a tool for distinguishing various cation site distribution models in iron titanium oxides. A small difference in cation distributions ($FeTi_2O_5$ versus $[Fe_{.9}Ti_{.1}][Fe_{.1}Ti_{1.9}]O_5$) yields significantly different neutron scattering lengths for the two pseudobrookite sites. As discussed above, this is due to the difference in the sign of the iron (0.95×10^{-12} cm) and titanium (-0.33×10^{-12} cm) neutron scattering lengths.

It is clear from the X-ray and neutron diffraction experiments that different cation distributions distinguish the high and low temperature pseudobrookite phases. Furthermore, since the scattering length of the *A* site has decreased and that of the *B* site has increased, it is reasonable that this change is a simple exchange of Ti from the *B* site to the *A* site with concurrent transfer of ferrous ions from the *A* to the *B* site. The high to low temperature phase changes are summarized below, for slag I,

$$(Mn_{0.05}Fe_{0.33}Ti_{0.52})(Ti_{2.00})O_5 \rightarrow (Mn_{0.05}Fe_{0.23}Ti_{0.62})(Ti_{1.9}Fe_{0.1})O_5$$

and for slag II;

TABLE II

RESULTS OF RIETVELD REFINEMENTS OF SLAG II AT DIFFERENT TEMPERATURES

Conditions	Pseudobrookite (*Cmcm*)		Titanium oxide ($P4_2/mnm$)		Iron
	Normalized scale factor	Unit cell	Normalized scale factor	Unit cell	Normalized scale factor
25°C	—	a = 3.7620 b = 9.7547 c = 9.9989	—	a = 4.5957 c = 2.9612	—
t = 0 1000°C	0.100	a = 3.769 b = 9.893 c = 10.138	0.474	a = 4.638 c = 2.992	0.0
t = 80 min 1000°C	0.098	a = 3.768 b = 9.891 c = 10.140	0.557	a = 4.639 c = 2.992	0.0
t = 160 min 1000°C	0.093	a = 3.767 b = 9.890 c = 10.142	0.620	a = 4.638 c = 2.992	0.022
t = 300 min 1000°C	0.093	a = 3.766 b = 9.888 c = 10.142	0.651	a = 4.639 c = 2.992	0.061
t = 450 min 1000°C	0.089	a = 3.766 b = 9.888 c = 10.142	0.669	a = 4.638 c = 2.992	0.082
t = 590 min 1000°C	0.093	a = 3.766 b = 9.888 c = 10.143	0.713	a = 4.638 c = 2.992	0.103
t = 810 min 1000°C	0.094	a = 3.766 b = 9.887 c = 10.142	0.719	a = 4.638 c = 2.992	0.096
Exp. end 25°C	—	a = 3.7497 b = 9.7718 c = 10.0177	—	a = 4.6000 c = 2.9619	—

Note. Estimated standard deviations in lattice parameters are 0.002–0.003 for data taken at 900°C and 0.0002–0.0004 for data taken at 25°C.

$$(Mg_{0.21}Fe_{0.33}Ti_{0.46})(Ti_{1.9}Mg_{0.1})O_5 \rightarrow (Mg_{0.21}Fe_{0.23}Ti_{0.56})(Ti_{1.8}Mg_{0.1}Fe_{0.1})O_5.$$

In other words, there has been a transition between an "ordered" structure (essentially 100% Ti on the B site) at 1700°C to a disordered structure at the lower temperature. The cation distributions suggested above are consistent with the observed neutron scattering lengths at elevated temperatures (see Table III for calculated scattering lengths for the cation distributions listed above).

The hypothesis that cation reordering occurs as the temperature is raised is further supported by observations made on materials synthesized at different temperatures. ^{57}Fe Mossbauer effect spectroscopy and neutron diffraction experiments (*1*) on slags I and II quenched from temperatures above 1700°C have indicated that the respective cation distributions were $(Mn_{0.05}Fe_{0.33}Ti_{0.52})(Ti_{2.00})O_5$ and $(Mg_{0.21}Fe_{0.33}Ti_{0.46})(Ti_{1.9}Mg_{0.1})O_5$, respectively. This is in contrast to Mossbauer effect experiments reported in the literature (*2*) that have been

TABLE III

NEUTRON SCATTERING LENGTHS[a] OF *A* AND *B* SITES IN PSEUDOBROOKITE (AB_2O_5) COMPOUNDS

Slag I			Slag II		
Conditions	*A* site	*B* site	Conditions	*A* site	*B* site
25°C, t = 0	0.09(1)	−0.33(1)	25°C, t = 0	0.26(1)	−0.29(1)
900°C, t = 0	−.06(2)	−0.28(2)	1000°C, t = 0	0.10(2)	−0.17(2)
900°C, t = 510 min	−.10(2)	−0.30(2)	1000°C, t = 810 min	0.14(2)	−0.17(2)
25°C, end	−.09(1)	−0.28(1)	25°C, end[b]	0.26(1)	−0.24(1)

Pseudobrookite composition	Model compound scattering lengths: *A* site	*B* site
$(Mn_{0.05}Fe_{0.33}Ti_{0.52})(Ti_{2.00})O_5$	0.12	−0.33
$(Mn_{0.05}Fe_{0.23}Ti_{0.62})(Ti_{1.9}Fe_{0.1})O_5$	0.00	−0.27
$(Mg_{0.21}Fe_{0.33}Ti_{0.46})(Ti_{1.9}Mg_{0.1})O_5$	0.27	−0.29
$(Mg_{0.21}Fe_{0.23}Ti_{0.56})(Ti_{1.8}Mg_{0.1}Fe_{0.1})O_5$	0.14	−0.22

[a] Scattering lengths are in units of 10^{-12} cm. Scattering lengths of Fe and Ti are 0.95×10^{-12} and -0.33×10^{-12} cm, respectively.

[b] Probably $(Mg_{.7}Ti_{.3})(Mg_{.2}Ti_{1.8})O_5$ with a trace of iron (see text).

performed on samples prepared at lower (1200°C) temperatures, in which ferrous ions were found in both *A* and *B* cation sites.

Structural characterization of titanium oxide compounds formed in the decomposition of pseudobrookite compounds. The cell constants of the titanium oxide phases formed from the decomposition of the slags (Tables I and II) are noteworthy in that they differ significantly from that of pure (i.e., TiO_2) rutile (a = 4.594(2), c = 2.959(2) Å) (*11*). The cell constants of the titanium oxide phases formed in the decomposition reactions are a = 4.6067(1) and c = 2.9653(1) Å for slag I, and a = 4.6000(1) and c = 2.9619(1) Å for slag II. These significant differences from the accepted values for TiO_2 prompted a refinement of the metal occupancy for each of these titanium oxide phases. The model which yielded the best fit to the observed neutron diffraction data for both slags I and II includes nuclear density at an interstitial (tetrahedral, $x = y = 0.167$, $z = 0.5$) site in the rutile structure. Because the refined scattering length of this site is positive, titanium is ruled out as occupying this site. Assuming that iron is located at this interstitial site, one possible stoichiometry of this phase (calculated from the refined scattering lengths of the atomic sites) is $Ti_{0.95}Fe_{0.025}O_{1.90}$ (hereafter referred to as "TiO_2"). This model includes the constraint that occupation of an interstitial tetrahedral site requires that two adjacent regular rutile octahedral sites be vacant due to their close proximity.

The possibility that ferrous ions exist within the titanium oxide phase was investigated by use of zero-field, ^{57}Fe Mossbauer effect spectroscopy. The Mossbauer effect data for slag samples I and II heated at 900 and 1000°C, respectively, are displayed in Figs. 8a and 8b, respectively. The spectrum for slag I is dominated by the six line magnetic hyperfine pattern due to the presence of elemental iron. The magnetic hyperfine pattern of elemental iron is also observed in the spectrum for slag II, which is, neverthe-

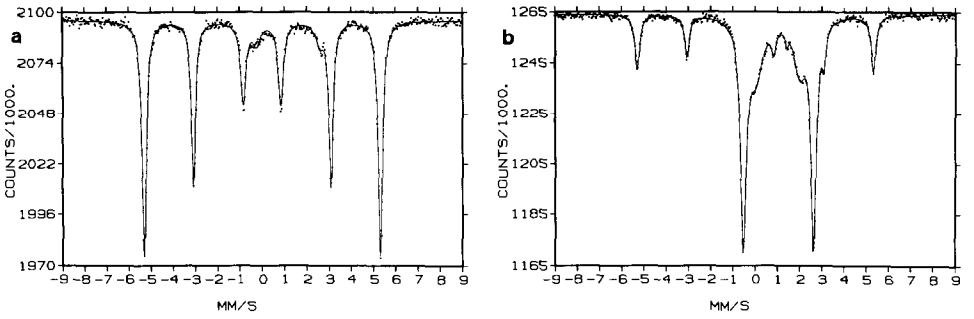

FIG. 8. Zero-field, natural abundance ^{57}Fe Mossbauer effect for (a) slag I and (b) slag II. Raw data are shown as points and the fit is shown as a solid line.

less, dominated by an intense quadrupole split doublet that is typical of high-spin ferrous ions in the fourfold sites of pseudobrookite, $FeTi_2O_5$ (*1*, *2*), in addition to a smaller quadrupole split doublet that is typical of high-spin ferrous ions in the eightfold sites of pseudobrookite. The resonances of a weak quadrupole split doublet typical of $FeTi_2O_5$ are also observed at ca. −0.3 and 2.6 mm/sec in the Mossbauer-effect data for slag I (Fig. 8a). The spectrum for slag I was nicely fit with one sextet (Fe) and one doublet ($FeTi_2O_5$); the pertinent curve fitting parameters are presented in Table IV. The small mole fraction of ferrous pseudobrookite remaining in slag I after high temperature decomposition, combined with the low population of ferrous ions believed present in the eightfold site of this material, precludes the direct observation of this signal in the Mossbauer spectrum. The ^{57}Fe Mossbauer effect "difference spectrum" (experimental data minus the fitted data) did not reveal any features of either structural or statistical significance. In view of the small fraction of Fe^{2+} postulated to occupy interstitial sites of rutile ($Ti_{0.95}Fe_{0.025}O_{1.90}$) and the interferences from the resonances due to Fe and $FeTi_2O_5$, it was not possible to substantiate the siting of ferrous ions at tetrahedral inter-

TABLE IV

RESULTS OF LEAST-SQUARES FITS OF LORENTZIAN LINE SHAPES TO ^{57}Fe MOSSBAUER EFFECT DATA[a]

	Pseudobrookite sites				Other sites			
Slag	Isomer shift[b]	Quadrupole splitting	FWHM	Area %	Isomer shift[b]	Quadrupole splitting	FWHM	Area %
I	1.17	2.83	0.41	7	0.00	0.00 (Fe)	0.25	93
II	1.05	3.15	0.30	50	0.00	0.00 (Fe)	0.26	22
	1.02	1.96	0.70	27				
					1.10	0.59 ($FeTiO_3$)	0.24	1

[a] Units for isomer shift, quadrupole splitting, and FWHM line widths are millimeters per second. Estimated standard deviations for these parameters are 0.02 mm/sec. Estimated standard deviation for the area percentage is 5%.

[b] All isomer shifts are relative to natural iron, α-Fe, at room temperature.

stices with the available Mossbauer effect data for slag I. Similarly, for slag II, the combination of the aforementioned interferences with those from the unresolved resonances between ca. 0.8 and 1.4 mm/sec that are typical of ferrous ions in ilmenite, $FeTiO_3$, (*12*), may obscure weak resonances due to Fe^{2+} ions at tetrahedral interstitial sites in rutile. The Mossbauer effect data for slag II were well-fit with one sextet (Fe) and three doublets ($FeTi_2O_5$ with Fe^{2+} in the four- and eightfold sites (*1*, *2*) and $FeTiO_3$). The results of the curve fitting analysis are summarized in Table IV. There were no significant peaks observed in the Mossbauer effect difference spectrum.

Chemistry of decomposition of iron titanium oxides. The nonoxidative decomposition of ferrous titanium oxide phases of the pseudobrookite structure can vary depending upon the iron/titanium ratio as well as the presence of nonferrous cations in the material. Three highly idealized potential modes are illustrated below:

$$FeTi_2O_5 \rightarrow FeTiO_3 + TiO_2 \quad (3)$$

$$2Fe_{0.5}Ti_{2.5}O_5 \rightarrow Fe + 5TiO_2 \quad (4)$$

$$4M_{0.3}Ti_{2.7}O_5 \rightarrow 2M_{0.5}Ti_{2.5}O_5 + 5Fe_{0.04}Ti_{1.16}O_2 \quad (M = Fe^{2+}, Mg^{2+} Mn^{2+}) \quad (5)$$

The first mode (Eq. (3)) may be operative in iron-rich materials and reflects the thermodynamic instability of pseudobrookite with respect to ilmenite and rutile (*3*). The second decomposition mode (Eq. (4)) may be operative for samples with a titanium/iron ratio of 5 and recognizes the thermodynamic instability of Fe^{2+} and Ti^{3+} with respect to Fe^0 and Ti^{4+} (*4*). The third mode (Eq. (5)) may be observed in very titanium-rich phases and allows for the possibility that ferrous ions may be found in a rutile-like titanium oxide phase. The reactant and product pseudobrookite phases in Eq. (5) are assumed to coexist in solid–solution. The eventual fate of the pseudobrookite phase produced in Eq. (5) depends upon the cation identity. Pseudobrookite phases rich in Mg^{2+} are stable, whereas ferrous-rich phases will decompose according to Eq. (4). Additional decomposition pathways that include the formation of other reduced titanium oxides (Ti_nO_{2n-1}) could also be included as possible reaction modes.

The kinetics of the decomposition of the pseudobrookite phases of slags I and II are illustrated in Figs. 9 and 10, respectively. Tables I and II contain cell constant and other information gained from Rietveld analyses as a function of time at 900 and 1000°C. Examination of Tables I and II indicates that the only products of decomposition are titanium oxide and iron. This is confirmed by ^{57}Fe Mossbauer effect spectroscopy. The Mossbauer effect spectra of slags I and II taken at the conclusion of the high temperature experiments show resonances due to iron metal and unreacted ferrous pseudobrookite. There were no other iron-bearing components in slag I. For slag II, the Mossbauer-effect data also revealed small concentrations of ilmenite that were identical to the phase distribution in the starting slag. Based on these findings, Eq. (3) (ilmenite production) can be eliminated as a decomposition mode in these slag samples.

The cell constants of the pseudobrookite phases also vary during the pseudobrookite decomposition. For slag I, unit cell parameters (Table I) are essentially constant from 0 to 180 min and then change slightly and gradually from 180 to 510 min. For slag II (Table II) the situation is reversed; from 0 to 160 min a slight change in unit cell parameters is noted, whereas for the time period 300 to 810 min the cell constants do not change. For both I and II the overall change in cell parameters is confirmed by comparing the more precise lattice parameters derived from the room temperature data taken before and after the decomposition experiment. Changes in these parameters indicate that the compositions of the pseudobrookite

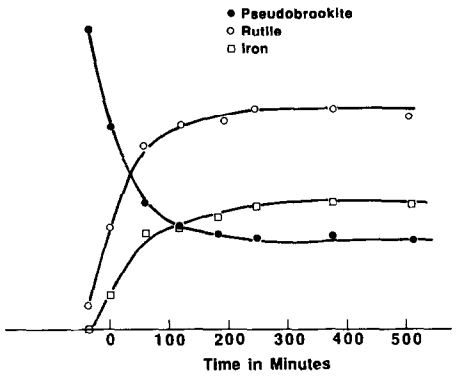

FIG. 9. The scale factors from Rietveld refinements of three phases, iron, titanium dioxide, and pseudobrookite for slag I at 900°C are plotted versus time. Note the continuous nature of the change in scale factors. This supports the suggestion that one single decomposition manifold is operable. Scale factors are directly proportional to relative mole fractions ($X = SZV$ where S = scale factor, V = unit cell volume, and $Z = 2$ for TiO_2, $Z = 4$ for M_3O_5, and $Z = 4$ for iron metal).

phases for slags I and II vary during the decomposition. This is confirmed by the observed scattering lengths of the two cation sites in the pseudobrookite structures: they also vary as a function of time at elevated temperatures.

In Figs. 9 and 10, the normalized scale factors for each phase resulting from Rietveld refinements of each data set taken at elevated temperatures (see Tables I and II) are plotted as a function of time. Because the scale factors are proportional to the mole fractions of each phase (9), these plots quantify the appearance and disappearance of products and reactants, respectively.

A discontinuity in Fig. 10 (slag II) indicates that at least two processes occur during decomposition of this sample. From 0 to approximately 160 min, a decomposition mode that produces only a metal oxide (MO_{2-x}) whose parameters are consistent with titanium oxide with the rutile structure is in evidence. During this first 160 min the decomposition of slag II is modeled by Eq. (5), wherein an iron-doped, oxygen-deficient titanium dioxide is the only product. Also, the variation of cell constants with time reflects an increase in Fe content of the remaining pseudobrookite phase. After this 160-min induction period, iron metal appears as a product in addition to titanium oxide, and the rate of disappearance of the pseudobrookite phase decreases sharply. Calculating the increase in the mole fractions (9) of iron metal and titanium oxide during this time frame (160–810 min) indicates that the titanium oxide phase content of the sample has increased about five times that of the iron. This behavior is best modeled by Eq. (4), wherein iron and rutile are produced at a ratio of 1 : 5. This is also supported by the lack of change of cell parameters for the pseudobrookite phase during this time period. Decomposition according to Eq. (4) does not produce a pseudobrookite phase of differing composition.

No corresponding discontinuity is observed in Fig. 9 (slag I), and during the course of the decomposition reaction, both an iron-doped, oxygen-deficient titanium di-

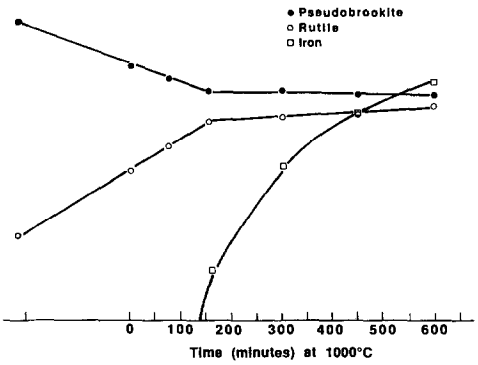

FIG. 10. The scale factors from Rietveld refinements of three phases, iron, titanium dioxide, and pseudobrookite, for slag II at 1000°C are plotted versus time. Note the discontinuity at 160–180 min. This supports the suggestion that two decomposition modes are utilized in this reaction. Conversion of scale factors to mole fractions is described in the legend to Fig. 9.

oxide and iron metal are formed continuously. We ascribe this behavior to the occurrence of a reaction modeled by a combination of Eqs. (4) and (5).

The difference in decomposition between I and II can be rationalized by recognizing their different cation composition. Slag II, which contains a significant amount of Mg, will decompose to iron metal and "TiO_2," until a Mg^{2+}-rich phase results. At that point, decomposition will be severely retarded (note that $MgTi_2O_5$ is stable under the reaction conditions employed here). This is the behavior observed (see Fig. 10). Conversely, slag I contains no Mg to stabilize the pseudobrookite phase at 900°C. This difference is reflected in the diffractograms of the products of decomposition. For I (Fig. 2) the Bragg data are largely due to Fe and "TiO_2," whereas for II (Fig. 4) a significant amount of a pseudobrookite phase remains. Assuming the remaining pseudobrookite phase (after 800 min at 1000°C) to be composed largely of magnesium and titanium oxides (a small amount of iron must be present to remain consistent with the Mossbauer data), the cation distribution corresponding to the scattering lengths given in Table III is $(Mg_{.7}Ti_{.3})(Mg_{.2}Ti_{1.8})O_5$.

Summary

Two distinct steps have been observed in the decomposition of metastable titanium-rich pseudobrookite phases ($M^{2+}_{1-x}Ti_{2+x}O_5$, M predominantly Fe and Mg) synthesized above 1700°C under reducing conditions. The first step involves a phase transition that occurs above 500°C from a high temperature, ordered structure to a low temperature, disordered pseudobrookite (AB_2O_5) phase. This order–disorder transition involves cation redistribution wherein ferrous ions are transferred from the A site to the B site (which previously contained no iron) and titanium is transferred from the B site to the A site. The second step observed is the low temperature phase decomposition of the disordered pseudobrookite structure to the reaction products. *In situ* neutron diffraction experiments, as well as ^{57}Fe Mossbauer effect spectroscopy, have been used to study the decomposition of the low temperature, disordered pseudobrookite phases. There are at least two manifolds of decomposition for these phases: the decomposition products are iron metal, and an iron-doped, oxygen-deficient titanium oxide (TiO_{2-x}) of the rutile structure.

The two step mechanism described above (cation distribution followed by decomposition) is worthy of further discussion. Recall that in the high temperature phase, ferrous cations are restricted to A sites within the pseudobrookite structure and that due to the three-dimensional structure, this isolates them from each other. It may not be coincidental that phase decomposition proceeds only after the ferrous ions are randomly distributed over all cation (A and B) sites. One mode of decomposition (Eq. (4)) involves electron transfer from Ti^{3+} to Fe^{2+},

$$2Ti^{3+} + Fe^{2+} \rightarrow 2Ti^{4+} + Fe^0, \qquad (6)$$

and the possibility that this reaction is kinetically allowed only when ferrous ions are distributed over all sites exists. This possibility will be the subject of future work.

Acknowledgments

The authors thank BP America and QIT-Fer et Titane, Inc. for permission to publish this work. The Intense Pulsed Neutron Source is a United States Department of Energy-operated user facility, contract No. W-31-109-ENG-38.

References

1. R. G. Teller, M. R. Antonio, A. E. Grau, M. Gueguin, and E. Kostiner, *J. Solid State Chem.* **88**, 334 (1990).
2. I. E. Grey and J. Ward, *J. Solid State Chem.* **7**, 300 (1973).
3. A. Navrotsky, *Amer. Miner.* **60**, 249 (1975).
4. I. Toromanoff and F. Habashi, *J. Less-Common Met.* **97**, 317 (1984).

5. R. A. YOUNG, NBS Spec. Publ. 567 (1979) and references therein.
6. R. J. HILL, *Acta Crystallogr. Sect. A* **45,** FGC19 (1989).
7. (a) J. R. HAUMAN, R. T. DALEY, T. G. WORLTON, AND R. K. CRAWFORD, *IEEE Trans. Nucl. Sci.* **NS-29,** 62 (1982); (b) R. B. Von Dreele, J. D. Jorgensen, AND C. G. Windsor, *J. Appl. Crystallogr.* **15,** 581 (1982); (c) J. D. Jorgensen and J. Faber, "ICANS-II, Proc. VIth Int. Collab. Adv. Neutron Sources, Argonne Natl. Lab., June 28–July 2, 1982," ANL-82-80 (1983).
8. (a) PAULING, L. *Z. Kristallogr.* **73,** 97 (1930); other models have also been proposed for pseudobrookite, such as (b) S. MURANAKA, T. SHIRJO, Y. BANDO, AND T. TAKODA, J. *Phys. Soc., Japan,* **30,** 890 (1971); (c) M. HAMMELIN, *Soc. Chim., France Bull.* **5,** 1559 (1958); (d) J. R. SMYTH, *Earth Planet. Sci. Lett.* **24,** 262 (1974); (e) B. A. WECHSLER, *Amer. Miner.* **62,** 913 (1977). In the ensuing discussion, the term pseudobrookite will be used to describe a structure type adopted by some oxides of the M_3O_5 composition.
9. (a) R. J. HILL AND C. J. HOWARD, *J. Appl. Crystallogr.* **20,** 467 (1987); (b) D. L. BISH AND S. A. HOWARD, *J. Appl. Crystallogr.* **21,** 86 (1988).
10. G. J. LONG, T. E. CRANSHAW, AND G. LONGWORTH, *Mossbauer-Effect Reference Data Journal,* **6,** 42 (1983).
11. F. A. GRANT, *Rev. Mod. Phys.* **31,** 646 (1959). Unit cell parameters are $a = 4.594(3)$ and $c = 2.959(2)$ Å.
12. T. C. GIBB, N. N. GREENWOOD, AND W. TWIST, *J. Inorg. Nucl. Chem.* **31,** 947 (1969).